Ceramics International xxx (xxxx) xxx

Contents lists available at ScienceDirect

Ceramics International

journal homepage: www.elsevier.com/locate/ceramint

Versatile binder system as enabler for multi-material additive manufacturing of ceramics by vat photopolymerization

Johannes Schubert *, Chantal-Liv Lehmann, Frederik Zanger

wbk Institute of Production Science, Karlsruhe Institute of Technology (KIT), Kaiserstraße 12, 76131, Karlsruhe, Germany

ARTICLE INFO

Handling Editor: Dr P. Vincenzini

Keywords:
Binder development
Multi-material additive manufacturing (MMAM)
Slurry
Vat photopolymerization

ABSTRACT

Vat photopolymerization is an additive manufacturing process for producing ceramics with high printing resolution. Extending this approach to multi-material additive manufacturing, the aim is to combine two or more different ceramics in a single component to aggregate their advantages. For this, binders for different ceramic materials are required. To enhance the debinding step, this work aimed to develop a versatile binder system suitable for different ceramic materials. Finally, a binder system was developed and qualified for several different ceramic materials. By thermogravimetrical analyses, a suitable temperature curve for debinding was derived. In a final sintering step, the components were densified almost defect-free. Therefore, this work serves as an enabler for multi-material vat photopolymerization.

1. Vat photopolymerization of ceramics

Ceramics find widespread applications owing to their outstanding characteristics, such as high hardness and strength, high fracture toughness, chemical stability and high-temperature performance [1]. Since conventional manufacturing methods have limitations regarding the possible design freedom and individualization, additive manufacturing (AM) of ceramics has seen tremendous growth in recent years [2]. For example, vat photopolymerization (VPP) has already reached industrial readiness for series production, enabling the high-precision production of complex and individualized ceramic components [3,4]. To adapt their properties to the requirements and to enable further applications, new process approaches deal with the combination of different materials in a single component, so called multi-material additive manufacturing (MMAM) [5,6].

In vat photopolymerization, layers of a photosensitive slurry, a suspension of ceramic powder and a reactive binder system, are cured by selective application of light. To do so, small layers of slurry are applied on top of a glass vat and the building platform is immersed into the slurry from above. By spatially selective exposure, the slurry hardens at the exposed areas and adheres to the build platform. By repeating these steps, the component is built up layer by layer. It is initially in the so-called green state, i.e. it still contains the binder necessary for shaping. This is removed in a subsequent debinding step. In a final sintering step, the component obtains its characteristic properties and undergoes a corresponding volume shrinkage to close the porosity created by debinding [2].

Ceramic VPP slurries must meet a number of requirements in order to be used in the process. Firstly, a sufficiently high curing depth is required to guarantee a connection of the individual layers [7]. Secondly, a low viscosity is required to apply sufficiently thin layers of the slurry in the VPP machine [8]. As a third main requirement, a high ceramic filler content is needed to enhance the debinding, to reduce the volume shrinkage during sintering and therefore, to obtain higher component densities and a better dimensional accuracy [9]. Additionally, a low light scattering behavior, i.e. a high printing resolution [10], an adequate green strength [11] and a sufficient stability of the slurry [12] are required. Light-curing slurries for VPP are composed of ceramic particles and a binder system, generally consisting of photoinitiators, monomers, oligomers and optional additives [2,4]. In Refs. [4,13], several compositions of binders for different ceramic powders are summarized exemplarily. Most of them are based on acrylate-based monomers and possess material- and composition-dependent a ceramic loading of 40–60 % volume share. However, it has been shown that the same mixture cannot be transferred to other slurries with different ceramic powders or monomer solutions [4,13]. Therefore, it is necessary to test and to optimize the composition and the process parameters for each ceramic individually, considering the material-specific constraints and characteristics [4,13].

In multi-material VPP, at least two materials are combined in a single

* Corresponding author.
E-mail address: johannes.schubert@kit.edu (J. Schubert).

https://doi.org/10.1016/j.ceramint.2024.10.006
Received 5 June 2024; Received in revised form 17 September 2024; Accepted 1 October 2024
Available online 5 October 2024

component to adjust its properties locally. For example, hard and ductile, heat/electrically conductive and insulating, porous and dense or bioresorbable and bioinert materials can be combined [14]. To do so, at least two slurries are used in a special multi-material VPP machine, e.g. a 2M30 (Lithoz, Vienna, Austria).

For manufacturing multi-material components, the slurries must initially fulfill the requirements and restrictions of the monolithic VPP process [15], especially in terms of the printing process, e.g. a sufficiently high curing depth and a suitable viscosity [4]. Besides the printing process, the sintering of composite parts, the so-called co-sintering, is a major challenge, especially in terms of the chemical compatibility, the coefficient of thermal expansion and the preferred sintering conditions of the individual materials, which have to match in a co-sintering process [6]. A frequently underestimated step along the VPP process chain is the thermal debinding step, in which the binder required for shaping is eliminated by heating the green part in an oven. In this stage, the majority of the components' defects, especially delaminations and cracks, are initiated [16]. The slurry composition heavily influences the debinding process [17]. On the one hand, the ceramic content of the slurry should be as high as possible in order to keep the amount of binder to be removed as low as possible [18]. On the other hand, a high solid loading generally leads to higher viscosities [4]. Therefore, the interactions along the process chain have to be considered and the temperature profile for debinding has to be precisely adjusted [16,19]. Regarding multi-material VPP, an identical or at least very similar binder system for different ceramics has enormous advantages. This enables the knowledge gained from monolithic manufacturing to be largely transferred and the process parameters to be set precisely.

2. Materials and methods

2.1. Feedstock material and composition

Based on pertinent literature, e.g. Refs. [4,7,20,21], potentially suitable substances for the binder system were selected (Table 1).

The photoinitiator Camphorquinone (CQ) was selected based on its absorbance spectrum matching the 460 nm wavelength of the VPP machine [22]. Based on preliminary experiments, IBOA, HDDA and ETMPTA showed the highest potential and were used in a volume ratio of 1:2:1 for the first set of experiments. Additionally, the solvent 1-Octanol and the additive Rheobyk were required for reducing the viscosity of the slurry.

For the selected ceramic powders, percentile values of the agglomerates' diameters (d_{10}, d_{50}, d_{90}) were determined by laser diffraction in a Sync (Microtrac Retsch, Haan, Germany) to confirm the information provided in the data sheet (Table 2). In the measurements, isopropanol was used as carrier liquid. Additionally, the particle sizes of the powders were determined by scanning electron microscopy in a JSM-6010 Plus (Jeol, Freising, Germany).

The initial development of the slurry was carried out on aluminum oxide. The results regarding the slurry composition were transferred to the other ceramics afterwards. The viscosity, the curing behavior and the curing depth of the slurries were determined to prove the general suitability for the VPP process. For Al_2O_3, ZrO_2, ATZ and ZTA, appropriate printing and debinding parameters were determined experimentally based on pre-defined sample geometries. Additionally, the parts were sintered exemplarily to prove the further processability of the green parts obtained by printing the prepared slurries. In Table 3, the use of the different ceramic powders for the different experiments is shown.

In a first set of experiments, the initiator system was optimized by adding different co-initiators and varying its share compared to the photoinitiator, while keeping the remaining slurry composition constant. The share of the initiator system in the binder was set to be sufficiently high with 12.5 vol-% (Table 4).

In a second set of experiments, the ratio of the three monomers IBOA, HDDA and ETMPTA was varied in a simplex centroid grid of grade 3 to identify the optimized composition. To do so, their common share in the slurry was kept at 32.6 mass-%, while maintaining the further composition constant, i.e. according to Table 4. Additionally, the best initiator system from the first set of experiments was used. Based on the results obtained, the share of the initiator system, the solvent, the additive and the monomers were varied purposefully to further optimize the slurry composition iteratively.

2.2. Machines and characterization

For preparing the slurries, a planetary centrifugal mixer Thinky ARE-250 (supplied by C3 Prozess-und Analysetechnik, Haar, Germany) was used. The mixing took place in three stages of 1 min at 2000 rpm, separated by 2 min for cooling purposes, each. To enhance the mixing performance, 20 aluminum oxide balls (diameter approx. 5 mm) were added before mixing. After mixing, the slurry was further homogenized in a three-roll mill Exakt 50i (Norderstedt, Germany) for 2 min with a minimum gap of the rollers below 10 µm.

The slurries were characterized at 20 °C on a Haake Mars 40 rheometer (ThermoFisher Scientific, Karlsruhe, Germany) with a connected Delolux 50 LED light source (DELO, Windach, Germany) by using a 20 mm plate-plate geometry. The wavelength of the light source is 460 nm and therefore, matches the used Lithoz 2M30 Science multi-material VPP machine. For matching the intensities of the light sources on the rheometer and the Lithoz VPP machine, both intensity profiles were

Table 1
Overview of the organic substances used, their function and supplier.

Name	Supplier	Function
Isobornyl acrylate (IBOA)	TCI Chemicals	Monomer (1 fct. group)
1,6-Hexanediol diacrylate (HDDA)	TCI Chemicals	Monomer (2 fct. groups)
Trimethylolpropane ethoxylate triacrylate (ETMPTA)	TCI Chemicals	Monomer (3 fct. groups)
Camphorquinone (CQ)	TCI Chemicals	Photoinitiator
4-(Dimethylamino) benzonitrile (4-DMABN)	TCI Chemicals	Co-Initiator
Ethyl-4 dimethylamino benzoate (E−4-DMAB)	TCI Chemicals	Co-Initiator
N-Phenylglycine (N-PG)	TCI Chemicals	Co-Initiator
Rheobyk	BYK-Chemie	Additive
1-Octanol	TCI Chemicals	Solvent

Table 2
Overview of the ceramic powders used, their supplier as well as their particle and agglomerate size.

Name	Supplier	Particle size	Agglomerate size in µm		
		in µm	d_{10}	d_{50}	d_{90}
Aluminum oxide (Al_2O_3)	Final Advanced Materials	0.3	0.28	1.306	6.28
Zirconium oxide (ZrO_2)	TOSOH	0.2	0.31	0.974	2.55
Alumina-toughened Zirconia (ATZ)	*20/80 mixture by weight of Al_2O_3 and ZrO_2*				
Zirconia-toughened Alumina (ZTA)	*80/20 mixture by weight of Al_2O_3 and ZrO_2*				
Silicon oxide (SiO_2)	Honeywell Chemicals	0.8	0.82	2.903	8.920
Titanium oxide (TiO_2)	Sigma-Aldrich	1	1.34	3.31	7.74
Aluminum nitride (AlN)	Final Advanced Materials	1	1.09	2.69	4.91

Table 3
Overview of the use of the ceramic powders in the different experiments.

Material	Initiator system and monomers	Slurry viscosity	Curing behavior and curing depth	Printing parameters	Debinding and sintering
Al_2O_3	X	X	X	X	X
ZrO_2		X	X	X	X
ATZ		X	X	X	X
ZTA		X	X	X	X
SiO_2		X	X		
TiO_2		X	X		
AlN		X	X		

Table 4
Generalized slurry composition of the first set of experiments performed using Al_2O_3.

Substance	Share (binder system)	Share (slurry)
IBOA	15.0 vol-%	8.3 vol-%
HDDA	30.0 vol-%	16.5 vol-%
ETMPTA	15.0 vol-%	8.3 vol-%
1-Octanol	20.0 vol-%	11.0 vol-%
Rheobyk	7.5 vol-%	4.1 vol-%
Initiator system	12.5 vol-%	6.9 vol-%
Al_2O_3	–	45.0 vol-%

evaluated at the position of the slurry to be cured by a Delolux Control photometer (DELO, Windach, Germany) and summarized in a look-up table prior to the experiments.

During slurry development, the viscosities of the slurry mixtures were exemplarily evaluated at a shear rate $\dot{\gamma} = 100\ s^{-1}$ on the rheometer in rotation mode. Additionally, the storage moduli of the individual mixtures G′ were determined in oscillation mode with a gap of 0.05 mm while exposing the slurries for 20 s with an intensity of 45 mW/cm^2 to enable a slow curing behavior and thus, a high measuring resolution. The measured G' was evaluated 30 s after the end of the exposure to guarantee a completed curing reaction. The measurements were performed 3 times each. The same parameters were also used in the series of experiments to determine the curing depth.

The evaluation of the curing depth was carried out by applying an approximately 2 mm thick layer of slurry on a glass plate with known thickness and uniform exposure with the Delolux light source. In order to capture uncured regions along the layer, a sufficiently long settling time of 60 s was awaited before removing the uncured slurry using a cotton swab soaked with isopropanol carefully. The thickness of the layer was measured by a micrometer Micromahr (Mahr, Göttingen, Germany). For comparison, the thickness was evaluated according to EN ISO 2808 by the wedge-cut approach using a byko-cut (BYK-Gardner, Geretsried, Germany).

In order to demonstrate the further processability of the slurries in the VPP machine and along the process chain, the further process steps were investigated for selected materials. Based on their technical relevance and widespread use, the materials Al_2O_3, ZrO_2, ATZ and ZTA were selected for this purpose (see also Table 3).

The evaluation of the design limitations was carried out by two sample print jobs (Fig. 1). Fig. 1a) shows a grid structure with overhanging bars (varying width from 0.4 to 4.8 mm; varying thickness from 0.2 to 1.0 mm) for evaluating the printing resolution in printing direction z and vertically overhanging bars. Fig. 1b) shows overhanging structures with angles ranging from 5° to 85° (max. cantilever length 10 mm). All parts were printed without support structures and all dimensions match a multiple of the pixel grid of the VPP machine, i.e. 40 µm. Starting from the parameters used in the curing depth experiments, optimized printing parameters were found by iterative adjustment of energy and intensity by evaluating the curing depth and the visible overcuring.

To evaluate the accuracy of the printing process, exemplary computed tomography (CT) measurements of zirconium oxide components with the geometry shown in Fig. 1a) were performed on a Metrotom 800 (Zeiss, Oberkochen, Germany). The setup included a 0.5 mm thick aluminum pre-filter, operating at 100 kV voltage and 80 µA current. The comparison of actual and target geometry was carried out using VGSTUDIO MAX 3.4.5 software (Volume Graphics, Heidelberg, Germany) by summing the absolute values of the deviation in all spatial directions.

To prove the suitability of the slurries for the whole VPP process chain, an investigation of the debinding was carried out by thermogravimetric analysis (TGA) of hollow cylinders (outer diameter 5 mm, wall thickness 1 mm, height 8 mm) on a STA 449 F1 Jupiter (Netzsch, Selb, Germany) with a heating rate of 1 K/min in air. Based on the results of the TGA analysis, a debinding process was performed in a GLO 10/11 (Carbolite Gero, Neuhausen, Germany) using cylinders (diameter 5 mm, height 10 mm). A subsequent sintering step of the samples was performed material-specifically at 1500 °C for ZrO_2 and at 1650 °C for ATZ, ZTA and Al_2O_3 with a holding time of 2 h in a HTF 1800 oven (Carbolite Gero, Neuhausen, Germany), each. Those parameters were derived based on pertinent literature, e.g. Refs. [23–25], and preliminary experiments. The densities of three samples per material were determined by applying the Archimedes principle in accordance with ISO 18754 using a precision scale XSR204 with density kit (Mettler-Toledo, Giessen, Germany) and distilled water as immersion fluid.

3. Results and discussion

3.1. Slurry development

Fig. 2 shows the influence of selected co-initiators and their share in the initiator system, consisting of the photoinitiator and one co-initiator, on the storage modulus after curing. It becomes apparent that the use of the pure photoinitiator CQ lead to a better result compared to the use of pure co-initiators showing the worst curing behavior. For E−4-DMAB and N-PG, a share of co-initiator in the range of 33–60 vol-% lead to similar values within the same initiator system, whereby the values for E−4-DMAB were almost one order of magnitude higher than the values

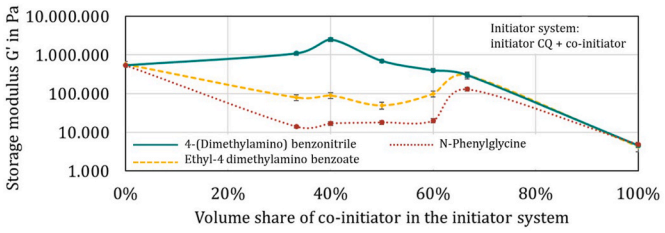

Fig. 2. Influence of different co-initiators and their share in the initiator system consisting of the photoinitiator CQ and the corresponding co-initiator on the storage modulus after curing.

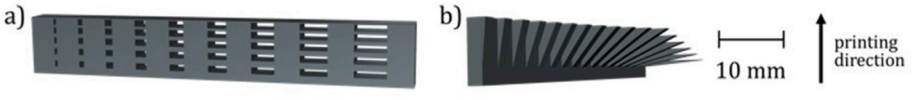

Fig. 1. Sample parts for evaluating a) the printing resolution in z-direction and vertical overhangs, b) max. possible overhanging angles.

for N-PG. For both co-initiators, highest storage moduli were obtained at a volume share of 67 %, but kept below the values of the pure photoinitiator CQ. The co-initiator 4-DMA-BN led to the highest storage moduli, i.e. the strongest curing, especially at a volume share of 40 %. The viscosity of the slurries was not significantly affected by the co-initiator variations. Therefore, a share of 40 % 4-DMA-BN in the initiator system was considered for the optimization of the monomers.

The better curing behavior of the pure photoinitiator CQ compared to the use of pure co-initiators can be explained by the bad light sensitivity of the co-initiators itself. The intermediate values for E−4-DMAB and N-PG at shares of 33–60 vol-% can be attributed to a reduced amount of CQ and a weak supporting effect of the co-initiator. For both co-initiators, the best results were obtained at a share of 67 %, which seems to be the optimized mixing ratio in these systems. Since the values of mixtures including those co-initiators are below the values of pure photoinitiator, they are less suitable. 4-DMA-BN showed the best performance, especially at a share of 40 % in the initiator system. This is in line with the results provided in Ref. [20], where the influence of different co-initiators was investigated on triethyleneglycol dimethacrylate. Therefore, 4-DMA-BN seems to be a relatively universal co-initiator for (meth) acrylate systems.

Fig. 3 shows a) the viscosity η and b) the storage modulus G' in dependency of the monomer mixture in a ternary plot. The results show that for mixtures with just one of the monomers IBOA, HDDA and ETMPTA, the viscosity and also the storage modulus after curing are increasing in the same order. This can be attributed to the functionality and the double bond density of the monomers. Generally, the higher the functionality and the double bond density of the monomer, the higher the viscosity and the stronger the bonding after curing [4].

Slurries with mixtures of different monomers possess viscosities between the viscosities of slurries with just one monomer. A mixture of IBOA, HDDA and ETMPTA showed a disproportionately high curing peak, while maintaining a relatively low viscosity. This can be attributed to an increased mobility of the free radicals and double bonds due to the proportion of the low-functional monomer, in this case IBOA, and the simultaneously stronger cross-linking effect of the higher-functional monomers, in this case HDDA and ETMPTA [21]. Therefore, the mixture of monomers with different functionality seemed to be a promising approach [4], which has also been confirmed in the experimental studies of this work.

Based on these results, the mixture composition was iteratively optimized by varying the individual shares selectively, to increase the ceramic share. Predominantly by adjusting the monomer composition and the additive, it was possible to eliminate the solvent share, i.e. 1-Octanol, and therefore, to increase the ceramic fraction. This can mainly be attributed to the low viscosity of IBOA.

Furthermore, the mixture composition is also transferred to other ceramic materials, especially to ZrO_2, ZTA, ATZ, TiO_2, SiO_2 and AlN. Table 5 summarizes the compositions of the processable slurries with the highest ceramic fractions obtained after optimization.

The results of the viscosity and curing analysis are given in Fig. 4. All slurries show a shear-thinning behavior with viscosities between 0.1 and 20 Pa s at a shear rate of 100 s^{-1}, whereby a shearing of the measuring geometry was sometimes be recognized at high shear rates, e.g. for TiO_2 and SiO_2. The slurry partially detached from the upper, rotating measuring geometry, so that a lower torque and consequently an apparently lower viscosity were recorded. Since the 2M30 VPP machine used has a rotating coating system, different shear rates are applied depending on the position within the vat. In the specific case of the 2M30 machine, this spans a shear rate range of approximately one order of magnitude. The adjustable rotation speed of the system allows the shear rate to be specifically adapted to the properties of the slurry. A particularly good shear rate range, i.e. with the lowest possible and most uniform viscosity, is kept white in Fig. 4a, and the less suitable areas are grayed out.

In general, the suspensions show for uniform deformation a constant level of G′ below 3500 Pa. After the exposure, G' increased for all ceramics values above 800,000 Pa.

By further iterative optimization, slurries with a similar binder system and ceramic filler contents of 56, 50, 50, 48.8, 46, 46 and 45 vol-% for Al_2O_3, ZTA, SiO_2, AlN, ZrO_2, TiO_2 and ATZ could be obtained at acceptable viscosities, which are within the range of the state of the art for material-specifically optimized slurries (see e.g. Refs. [4,13]).

3.2. Printing process

Table 6 shows the curing depths C_d obtained for the slurries cured for 20 s with an intensity of 45 mW/cm^2.

The results show that with the same exposure different material-specific curing depths are achieved. This is generally in line with the

Table 5
Composition of the optimized slurries for different ceramic materials (all shares in vol-%).

Substance	Al_2O_3	ZrO_2	ZTA	ATZ	TiO_2	SiO_2	AlN
IBOA	15.5	19.0	18.0	19.5	20.3	18.6	15.5
HDDA	15.5	19.0	18.0	19.4	16.1	14.3	14.5
ETMPTA	6.0	8.0	7.0	8.0	3.6	3.7	7.6
Rheobyk	3.0	2.4	2.0	2.4	7.6	4.5	1.8
CQ	3.0	4.0	3.5	4.1	4.3	5.6	7.7
4-DMA-BN	1.0	1.6	1.5	1.6	2.1	3.3	4.1
Ceramic	56.0	46.0	50.0	45.0	46.0	50.0	48.8

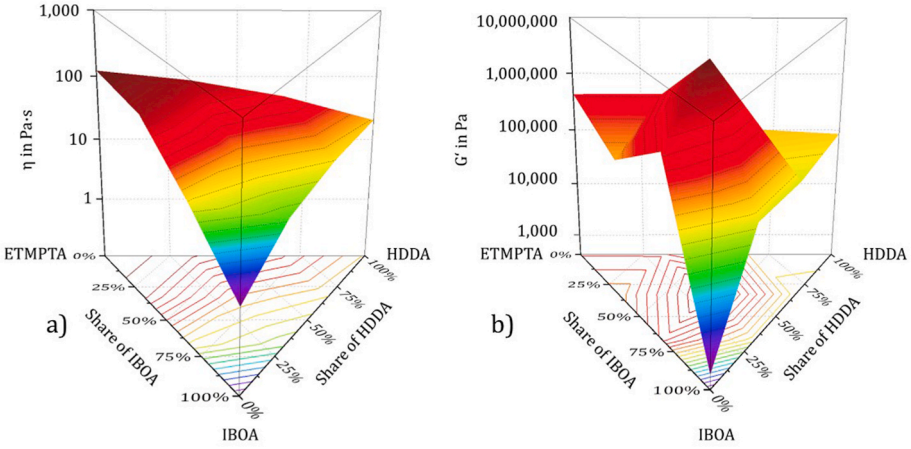

Fig. 3. Influence of the IBOA, HDDA and ETMPTA share on a) the viscosity at 100 s^{-1} and b) the storage modulus after curing.

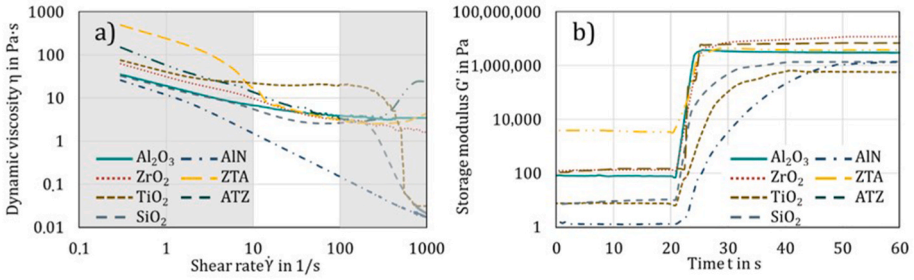

Fig. 4. Rheological analysis of the slurries: a) viscosity in dependency of the shear rate, b) storage modulus over time (exposure started at 20 s).

Table 6
Curing depth C_d of the slurries with an exposure time of 20 s and an intensity of 45 mW/cm.^{2}.

Slurry	Al_2O_3	ZrO_2	ZTA	ATZ	AlN	TiO_2	SiO_2
C_d in µm	358	106	239	153	32	57	452

increasing curing depth by reducing the refractive index difference Δn between binder system and the powder of oxide ceramics [4]. The refractive index of the binder system is based on [13] in the range of 1.45, leading to refractive index differences of 0.11, 0.318, 0.396, 0.430, 0.704, 0.738 and 1.164 for SiO_2, Al_2O_3, ATZ, ZTA, AlN, ZrO_2 and TiO_2, respectively [13,26–29]. Most of the variation in curing depth can therefore be attributed to the difference in the refractive index. Other differences are most likely due to the small variations in the composition of the binder system and material-specific interactions between initiators, monomers and the specific powders. Nonetheless, the results showed that curing depths greater than the minimum layer thickness of 10 µm required for processing in the VPP system could be achieved for all materials examined. The slurries are therefore generally suitable for processing in the VPP system. However, the results also show that a precise selection of exposure parameters was necessary for printing components successfully and for achieving a high resolution, e.g. higher energies were necessary for ATZ and ZTA in comparison to Al_2O_3.

Fig. 5 shows selected zirconium oxide parts printed with different parameters. The samples in Fig. 5 a) and b) were printed with an intensity of 80 mW/cm^2 and an energy of 105 mJ/cm^2, leading to a high printing resolution. In contrast, an increased curing energy of 150 mJ/cm^2 using the same intensity led to a massive overpolymerization (Fig. 5c). Despite the same binder system, different optimum printing parameters had to be found for each ceramic.

Fig. 6 shows a computer tomography (CT) measurement of a ZrO_2 part printed with a curing energy of 105 mJ/cm^2. A deviation chart was generated by comparing target and actual geometry. The measurement was conducted in a combined manner including the sum of the absolute values of the deviation in all spatial directions. The combination of both figures reveals deviations, especially in a range of 0 and 100 µm. Therefore, the actual geometry corresponds quite well to the target geometry. The existing deviations occur primarily on the larger surface area along the printed contour in y-direction. It is also evident on the overhanging bars, that there are larger deviations in z-direction, caused by the curing depths of more than 150 µm and delaminations of the thin layers.

In Table 7, appropriate printing parameters for Al_2O_3, ZrO_2, ZTA and ATZ are given.

In order to compensate the scattering effect shown in the CT measurement of a printed ZrO_2 part, a negative contour offset parameter can be applied, e.g. an adjustment by 40 µm can be used to reduce the part size along the contour by a total of 80 µm in the slicing process. The large deviation in the z-direction of the grid structures is due to the effect of delamination caused by the reduced number of exposures of the thin bars and the high curing depth of ZrO_2 compared to the layer thickness. To compensate for this effect, a z-parameter could be set, to extend the opening in build direction for a given layer count in the slicing process.

3.3. Debinding

Fig. 7 a) shows the results of the thermogravimetric analysis of Al_2O_3, ZrO_2 and ZTA parts. The actual debinding started at 100 °C and ended at approx. 450 °C. The major mass loss occurred between 230 and 400 °C, especially at 270 and 320 °C. There were just small deviations in mass loss between all tested materials. At the end of debinding, approx. 86.0, 85.2 and 85.0 mass-% of the ZrO_2, ZTA and Al_2O_3 samples are leftover, respectively. Based on the similar TGA curves, just one time-temperature profile for debinding actual parts was derived, where holding times were placed at temperatures with high mass loss to avoid debinding defects (Fig. 7 b). The debinding is followed by a short pre-sintering up to 1100 °C to increase the brown strength for handling purposes. This debinding approach enabled almost all parts to be debinded without visible defects.

The results of the TGA analysis are in line with the state of the art, e.g. Ref. [17]. The different mass of the components after debinding can be attributed to the varying binder shares and the different densities of the ceramic materials.

3.4. Sintering

For validation, the parts were sintered under material-specific sintering conditions, i.e. for 2 h at 1500 °C for ZrO_2, 1550 °C for ATZ as well as at 1650 °C for ZTA and Al_2O_3. Fig. 8 shows microsections of the three selected materials after sintering.

By Archimedean principle, densities of 98.8 %, 95.1 %, 95.2 % and 95.8 % were obtained for ZrO_2, ZTA, ATZ and Al_2O_3 after sintering, respectively. The results of the sintering experiments show the possibility to further process the components printed from the slurries along the process chain. The micrographs do not show any significant defects, such as delamination, so that it can generally be assumed that the process is suitable, in particular the debinding step. The densities of more than 95 % are promising for an initial sintering test. It becomes clear that

Fig. 5. Printed ZrO_2 parts: a) and b) with a curing energy of 105 mJ/cm^2 leading to a high printing resolution and c) with an energy of 150 mJ/cm^2 leading to a massive overpolymerization.

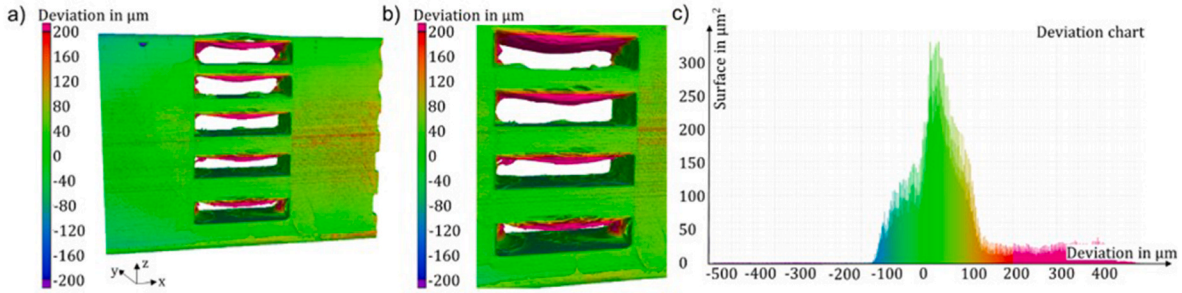

Fig. 6. a) Target-actual comparison, b) delaminations within the thin layers of the ZrO_2 part and c) deviation chart for a CT measurement of a ZrO_2 part printed with a curing energy of 105 mJ/cm.^{2}.

Table 7
Appropriate printing parameters for Al_2O_3, ZrO_2, ZTA and ATZ slurries.

Exposure parameter	Al_2O_3	ZrO_2	ZTA	ATZ
Intensity in mW/cm^2	80	80	80	80
Energy in mJ/cm^2	70	105	80	95

the selected sintering parameters were not equally suitable for the different materials. The parameters chosen for ZrO_2 at 1500 °C and a holding time of 2 h appear to be relatively well suited due to the density of almost 99 %. However, adjustments of the process parameters, especially regarding a co-sintering process of multi-material components are still to be investigated for the other materials. Nevertheless, the results and parameters of this study provide a good starting point, especially while considering the focus of this work being on the slurry development.

4. Conclusion

In this work, a versatile binder system consisting of the same constituents was developed as an enabler for multi-material vat photopolymerization. A common binder system is intended to prevent the formation of defects at material transitions, especially in the debinding step.

The main findings are:

- Development of slurries with the same constituents in the binder system and ceramic filler contents of 56, 50, 50, 48.8, 46, 46 and 45 vol-% for Al_2O_3, ZTA, SiO_2, AlN, ZrO_2, TiO_2 and ATZ fulfilling the requirements for VPP, i.e. acceptable viscosities and good curing behavior.
- The known correlation between curing depth and the refractive index difference Δn could generally be confirmed for oxide ceramics. Based on this, material-specific printing parameters were derived

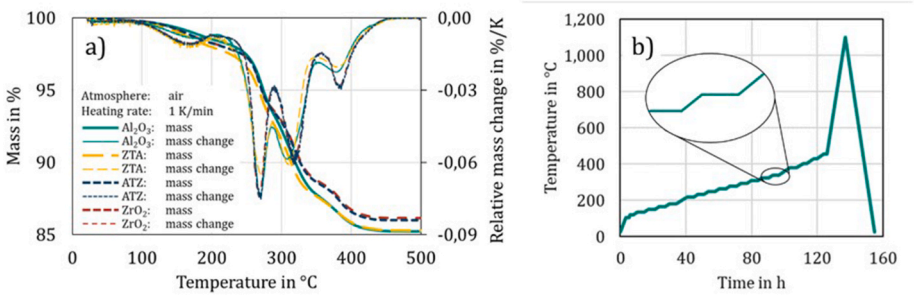

Fig. 7. a) Thermogravimetric analysis of Al_2O_3, ZTA, ATZ and ZrO_2 samples and b) derived temperature profile for debinding the parts in an oven.

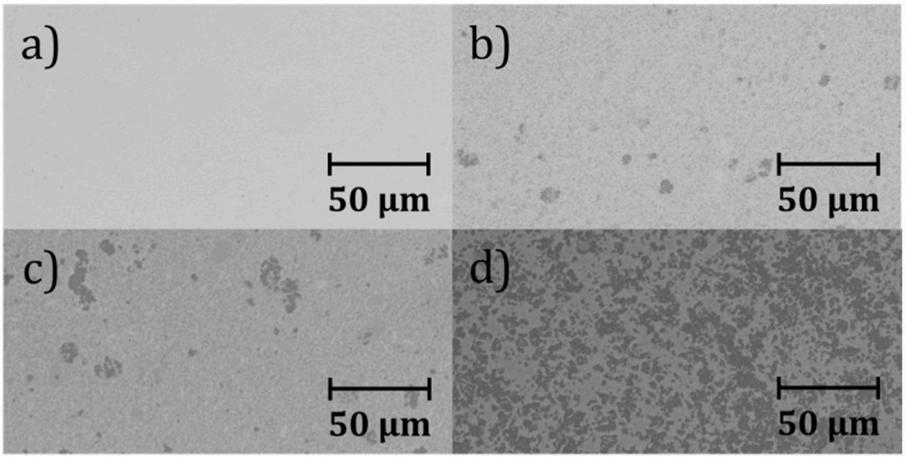

Fig. 8. Micrographs of samples sintered under material-specific sintering conditions: a) ZrO_2, b) ATZ, c) ZTA, d) Al_2O_3.

and the printing resolution exemplarily investigated by CT measurements.

- By TGA, a suitable debinding program for all binders was derived to debind the components without visible defects. Also, after sintering, no significant defects were observed.
- In initial sintering experiments, it could be proven that it is possible to further process the components printed from the slurries along the process chain, leading material dependent to densities between 95 % and almost 99 %, measured by Archimedean principle.

Overall, it can be concluded that the development of a versatile binder system being transferable and adaptable to different ceramics is a major step towards multi-material VPP. The results show the possibility to process the developed slurries along the further process chain leading to promising results, especially regarding the debinding step. Therefore, this paper serves as enabler for further research and the development of multi-material VPP process chains, pursuing uniform multi-material components with desired properties throughout all the necessary process steps.

CRediT authorship contribution statement

Johannes Schubert: Writing – review & editing, Writing – original draft, Visualization, Validation, Project administration, Methodology, Investigation, Formal analysis, Data curation, Conceptualization. **Chantal-Liv Lehmann:** Writing – original draft, Visualization, Validation, Methodology, Investigation, Formal analysis, Data curation. **Frederik Zanger:** Writing – review & editing, Validation, Supervision, Resources, Funding acquisition, Conceptualization.

Declaration of competing interest

The authors declare that they have no known competing financial interests or personal relationships that could have appeared to influence the work reported in this paper.

Acknowledgement

The authors would like to thank Jonas Brenneis and Sandro Schöner, Doriane Makiadi as well as Dr. Sandipan Sen for their support in the development of the slurries, the preparation of the microsections and the performance of the TGA analysis. The authors also would like to thank the Ministry of Science, Research and Arts of the Federal State of Baden-Württemberg for the financial support of the projects within the Innovation Campus Future Mobility (ICM).

References

[1] W. Kollenberg, Technische Keramik, Vulkan-Verlag, Essen, 2018.
[2] W. Kollenberg, Additive Fertigung Keramischer Komponenten, Vulkan-Verlag, Essen, 2020.
[3] U. Scheithauer, E. Schwarzer, T. Moritz, A. Michaelis, Additive manufacturing of ceramic heat exchanger: opportunities and limits of the lithography-based ceramic manufacturing (LCM), J. Mater. Eng. Perform. 27 (2018) 14–20, https://doi.org/10.1007/s11665-017-3087-1.
[4] S. Zakeri, M. Vippola, E. Levänen, A comprehensive review of the photopolymerization of ceramic resins used in stereolithography, Addit. Manuf. 35 (2020) 101177, https://doi.org/10.1016/j.addma.2020.101177.
[5] A. Nazir, O. Gokcekaya, K.M. Billah, O. Ertugrul, J. Jiang, J. Sun, S. Hussain, Multi-material additive manufacturing: a systematic review of design, properties, applications, challenges, and 3D printing of materials and cellular metamaterials, Mater. Des. 226 (2023) 111661, https://doi.org/10.1016/j.matdes.2023.111661.
[6] A. Michaelis, U. Scheithauer, T. Moritz, S. Weingarten, J. Abel, E. Schwarzer, W. Kunz, Advanced manufacturing for advanced ceramics, Procedia CIRP 95 (2020) 18–22, https://doi.org/10.1016/j.procir.2020.03.028.
[7] M.L. Griffith, J. Halloran, Freeform fabrication of ceramics via stereolithography, J. Am. Ceram. Soc. 79 (1996) 2601–2608, https://doi.org/10.1111/j.1151-2916.1996.tb08041.x.
[8] C.-J. Bae, A. Ramachandran, K. Chung, S. Park, Ceramic stereolithography: additive manufacturing for 3D complex ceramic structures, J. Korean Ceram. Soc. 54/6 (2017) 470–477, https://doi.org/10.4191/kcers.2017.54.6.02.
[9] W. Zimbek, R. Rice, Stereolithography of Ceramics and Metals, IS&T's 50th Annual Conference, 1997, pp. 649–655.
[10] T. Chartier, A. Badev, Y. Abouliatim, P. Lebaudy, L. Lecamp, Stereolithography process: influence of the rheology of silica suspensions and of the medium on polymerization kinetics – cured depth and width, J. Eur. Ceram. Soc. 32/8 (2012), https://doi.org/10.1016/j.jeurceramsoc.2012.01.025.
[11] H.-J. Lee, H.-Y. Park, E.-H. Kim, H.-H. Choi, J. Jin, J. Choi, S. Yang, Y.-G. Jung, Relationship between mechanical properties of ceramic green body and structures of photo-cured acrylate polymer for ceramic 3D printing based on photo polymerization, Ceram. Int. 47/3 (2021) 3867–3875, https://doi.org/10.1016/j.ceramint.2020.09.247.
[12] C.-J. Bae, J.W. Halloran, Concentrated suspension-based additive manufacturing – viscosity, packing density, and segregation, J. Eur. Ceram. Soc. 39/14 (2019) 4299–4306, https://doi.org/10.1016/j.jeurceramsoc.2019.05.034.
[13] I.L. de Camargo, M.M. Morais, C.A. Fortulan, M.C. Branciforti, A review on the rheological behaviour and formulations of ceramic suspensions for vat photopolymerization, Ceram. Int. 47 (2021) 11906–11921, https://doi.org/10.1016/j.ceramint.2021.01.019.
[14] S. Geier, I. Potestio, 3D-Printing: from multi-material to functionally-graded ceramic, Ceram. Appl. 8/2 (2020) 32–35.
[15] J. Schubert, C.-L. Lehmann, V. Schulze, F. Zanger, Potentials and challenges of multi-material additive manufacturing of ceramics by vat photopolymerization, Ceram. Appl. 11/3 (2023) 12–16.
[16] C.-J. Bae, J.W. Halloran, Influence of residual monomer on cracking in ceramics fabricated by stereolithography, Int. J. Appl. Ceram. Technol. 8/6 (2010) 1289–1295, https://doi.org/10.1111/j.1744-7402.2010.02559.x.
[17] E. Schwarzer-Fischer, J. Abel, J. Sieder-Katzmann, M. Propst, C. Bach, U. Scheithauer, A. Michaelis, Study on CerAMfacturing of novel alumina aerospike nozzels by lithography-based ceramic vat photopolymerization (CerAM VPP), Mater 15/9 (2022) 3279, https://doi.org/10.3390/ma15093279.
[18] W. Zimbeck, R. Rice, Stereolithography of ceramics and metals. IS&T Annual Conference, The Society for Imaging Science and Technology, 1997, pp. 649–655.
[19] H. Wu, Y. Cheng, W. Liu, R. He, M. Zhou, S. Wu, X. Song, Y. Chen, Effect of the particle size and the debinding process on the density of alumina ceramics fabricated by 3D printing based on stereolithography, Ceram. Int. 42/15 (2016) 17290–17294, https://doi.org/10.1016/j.ceramint.2016.08.132.
[20] J. Jakubiak, X. Allonas, J.P. Fouassier, A. Sionkowska, E. Andrzejewska, L. Linden, J.F. Rabek, Camphorquinone–amines photoinitating systems for the initiation of free radical polymerization, Polymer 44/18 (2003) 5219–5226, https://doi.org/10.1016/S0032-3861(03)00508-X.
[21] X. Xu, S. Zhou, J. Wu, Y. Liu, Y. Wang, Z. Chen, Relationship between the adhesion properties of UV-curable alumina suspensions and the functionalities and structures of UV-curable acrylate monomers for DLP-based ceramic stereolithography, Ceram. Int. 47/23 (2021) 32699–32709, https://doi.org/10.1016/j.ceramint.2021.07.200.
[22] T. Völkel, Wissenschaftliche Dokumentation bluephase Familie der Firma Ivoclar Vivadent, 2005.
[23] R. He, W. Liu, Z. Wu, M. Di An, M. Huang, H. Wu, Q. Jiang, X. Ji, S. Wu, Z. Xie, Fabrication of complex-shaped zirconia ceramic parts via a DLP- stereolithography-based 3D printing method, Ceram. Int. 44/3 (2018) 3412–3416, https://doi.org/10.1016/j.ceramint.2017.10.215.
[24] O.Y. Zadorozhnaya, T.A. Khabas, K. Kamyshnaya, V.A. Kutugin, S.E. Malykhin, Effects of sintering curves on microstructure, physical and mechanical properties and on low temperature degradation of zirconia-toughened alumina, J. Eur. Ceram. Soc. 41/16 (2021) 274–281, https://doi.org/10.1016/j.jeurceramsoc.2021.03.048.
[25] U. Scheithauer, E. Schwarzer, T. Moritz, A. Michaelis, Additive manufacturing of ceramic heat exchanger: opportunities and limits of the lithography-based ceramic manufacturing (LCM), J. Mater. Eng. Perform. 27/1 (2018) 14–20, https://doi.org/10.1007/s11665-017-3087-1.
[26] I.H. Malitson, M.J. Dodge, Refractive index and birefringence of synthetic sapphire, J. Opt. Soc. Am. 62/1 (1972), https://doi.org/10.1364/JOSA.62.001336, 1336–1336.
[27] J. Pastrňák, L. Roskovcová, Refraction index measurements on AlN single crystals, Phys. Status Solidi 14/1 (1966) K5–K8, https://doi.org/10.1002/pssb.19660140109.
[28] D.L. Wood, K. Nassau, Refractive index of cubic zirconia stabilized with yttria, Appl. Opt. 21/16 (1982) 2978–2981, https://doi.org/10.1364/AO.21.002978.
[29] J.R. Devore, Refractive indices of rutile and sphalerite, J. Opt. Soc. Am. 41/6 (1951), https://doi.org/10.1364/JOSA.41.000416.